

Research Article

A Lightweight Hybrid Dilated Ghost Model-Based Approach for the Prognosis of Breast Cancer

Edwin Ramirez-Asis ¹, Romel Percy Melgarejo Bolivar ², Leonid Alemán Gonzales ²,
Sushovan Chaudhury ³, Ramgopal Kashyap,⁴ Walaa F. Alsanie,^{5,6} and G. K. Viju ⁷

¹Universidad Nacional Santiago Antunez de Mayolo, Huaraz, Peru

²Faculty of Statistical Engineering and Computer Science, Computer Science Research Institute, National University of the Altiplano of Puno, P.O. Box 291, Puno, Peru

³University of Engineering and Management, Kolkata, India

⁴Amity University Chhattisgarh, Chhattisgarh, India

⁵Department of Clinical Laboratory Sciences, The Faculty of Applied Medical Sciences, Taif University, Taif, Saudi Arabia

⁶Centre of Biomedical Sciences Research (CBSR), Deanship of Scientific Research, Taif University, Taif, Saudi Arabia

⁷Post Graduate Studies, University of Garden City, Khartoum, Sudan

Correspondence should be addressed to Sushovan Chaudhury; sushovan.chaudhury@gmail.com and G. K. Viju; prof.gkviju@ugc.edu.sd

Received 28 April 2022; Revised 3 July 2022; Accepted 18 July 2022; Published 25 August 2022

Academic Editor: Vijay Kumar

Copyright © 2022 Edwin Ramirez-Asis et al. This is an open access article distributed under the Creative Commons Attribution License, which permits unrestricted use, distribution, and reproduction in any medium, provided the original work is properly cited.

Most approaches use interactive priors to find tumours and then segment them based on tumour-centric candidates. A fully convolutional network is demonstrated for end-to-end breast tumour segmentation. When confronted with such a variety of options, to enhance tumour detection in digital mammograms, one uses multiscale picture information. *Enhanced segmentation precision*. The sampling of convolution layers are carefully chosen without adding parameters to prevent overfitting. The loss function is tuned to the tumor pixel fraction during training. Several studies have shown that the recommended method is effective. Tumour segmentation is automated for a variety of tumour sizes and forms postprocessing. Due to an increase in malignant cases, fundamental IoT malignant detection and family categorisation methodologies have been put to the test. In this paper, a novel malignant detection and family categorisation model based on the improved stochastic channel attention of convolutional neural networks (CNNs) is presented. The lightweight deep learning model complies with tougher execution, training, and energy limits in practice. The improved stochastic channel attention and DenseNet models are employed to identify malignant cells, followed by family classification. On our datasets, the proposed model detects malignant cells with 99.3 percent accuracy and family categorisation with 98.5 percent accuracy. The model can detect and classify malignancy.

1. Introduction

In classic tumour segmentation studies, grey-level and texture indicators are utilised to divide mammograms into regions based on manually selected seed locations or small areas of dubious land [1]. Breast tumours are segmented using Gaussian filtering and mathematical morphological techniques [2]. The number of original segmented basins

was lowered by preprocessing. The active contour model [3, 4] divides breast masses into segments. To create an initial contour closer to the lesion border, region-growing segmentation is used. They use active contour 3D level-set segmentation and 3D radial gradient index segmentation [5]. Many approaches use vector-valued contours to segment mammographic masses. The first restrictions on smoothed mammograms were made using a level-set

method to improve the accuracy of segmentation. It takes less time to extract features from a pretrained DenseNet-121 model than it does to train a CNN model from scratch [6].

Another approach is deep network supervised segmentation. To develop a structured output and segmentation, learning employs a priori mass placement, size, and form. To improve segmentation performance, a CNN output is added to the potential functions. There are three phases of training. It displayed a network of bulk ROI images from start to finish [7]. CRFs were made for structured learning, and adversarial training was made for learning from sparse mammograms. CNN is used to classify images [8], detect objects, and segment images [9, 10], among other things. CNN-based image segmentation algorithms can separate pixels in a picture. The fully connected network (FCN) refined it using the VGG-Net [11]. Convolutional layers, rather than entirely connected layers, segment the classification network. In addition, FCN employs the skip architecture to improve segmentation results by mixing semantic and detailed data. Deconvolution has now become a standard in semantic segmentation [5]. Convolution was utilised in SegNet [12] to supplement sparse feature maps. U-Net [13] improved segmentation performance by combining upsampling output with encoding high-resolution features.

These results are based on the semantic segmentation extension of DenseNet [14]. Traditional CNN-based segmentation designs require end-to-end encoder-decoder training. An upsampling route is trained using the downsampling approach. Segmenting digital mammograms takes longer since they are bigger. Most unsupervised techniques need a priori characteristics such as starting seed locations and initial outlines. The accuracy of segmentation is affected by hand-crafted features and initial priori location. The grey value of internal and exterior tumour regions, for example, varies somewhat. *Formalised*. The tumour-centric candidate box is used in these procedures. Certain supervised segmentation algorithms know in advance the location, size, and form of the tumour. This is due to the inability of large objects to be divided directly. In addition to the tumour-centric rectangular zone, our proposed technique has the potential to segment the whole digital mammography picture. The proposed lightweight model uses skip connections in the upsampling route to assist the downsampling route in restoring spatial information. It outperforms prior findings with no pretraining or postprocessing. As a result, we enhanced DenseNet to separate tumours.

Our suggested strategy outperforms previous methods in our digital mammography dataset. For the rest of the paper, Section 2 is an overview of related work. The proposed model is explained in Section 3. The results of the dataset are summarised in Section 4. Section 5 concludes.

2. Related Work

To restore the input resolution, FC-DenseNet [15] offers an upsampling path. FC-DenseNet is made up of dense blocks and transition layers. DenseNet is composed of three similar convolutions with probability dropout (no resolution loss). A transition down layer is made up of 1-1 convolution

(saving feature maps) and 2-2 pooling. Each layer is an upsample. The feature maps that have been upsampled and downsampled are merged to form a new dense block input. A dense block's input and output are not concatenated. As demonstrated in Figure 1, the height and breadth of a malignant tumour are usually scattered between 200 and 800 pixels. Inaccurate segmentation might be a concern. Obtaining multiscale imaging data enhances the accuracy of tumour segmentation. In this method, pretrained DenseNet-121 is used to extract features. It uses the improved DNN-based feature categorisation model as input. Trainable weight layers in nonbatch normalisation layers 121. There are three transition layers and an initial convolutional layer. In the absence of a classifier, the DenseNet-121 [16] weights are loaded. It creates a volume form, which is then input into the fine-tuned DNN-based feature categorisation. It increases CNN performance and is derived from DenseNet-121 [16]. DenseNet contains fewer parameters than typical CNNs, resulting in a reduction in hyperparameters. It eliminates the need to memorise unneeded feature maps. The network's feature maps stay constant as the number of filters varies. The fading gradient issue has been mitigated. DNN-based feature categorisation has been improved.

As a result, all parallel CNN layers must compute scaled input characteristics. Different convolution kernel sizes can be used to extract multiscale visual characteristics [17, 18]. The size of the convolution kernel is an essential element in the feature extraction process. If a single convolution kernel is unable to adequately extract all the key features from a complex image, certain critical properties will be lost. These characteristics include to mention a few: as a result, a novel multiscale technique was developed. This approach employs many convolution kernels, allowing it to collect features at a wide range of scales. The smaller kernels in this experiment were all derived from the initial large-scale kernel. Convolution kernels of varied sizes broaden the network and improve the learning parameters. Less data mean greater overfitting. Extracting multiscale visual attributes requires many fields of view. The spatial pyramid pooling model collects multiscale image data, separates the input picture into spatial bins, and pools them. The output dimension of each spatial bin is uniform. As a result, the layer increases recognition accuracy. During the pooling process, image properties and geolocation data are lost.

The network receptive field is enlarged by atrous (dilated) convolution [19]. When using consecutive dilated convolutions, the receptive field expands exponentially, while the number of parameters rises linearly. If you want to quickly increase your sensitivity, we check out dilated convolutions and pooling approaches. Figure 2 depicts atrous convolution using a standard hole filter with zero-hole weights. Atrous convolution with rate increases the kernel of a filter without adding parameters. Every pixel in the input may be convoluted using atrous convolution. Contouring the network's receptive field without the use of parameters or calculations, may be used to widen filter fields at any network layer. The receptive field and sampling rates of a convolution kernel are used to aggregate the network features. Spatial pyramid pooling is employed to resample

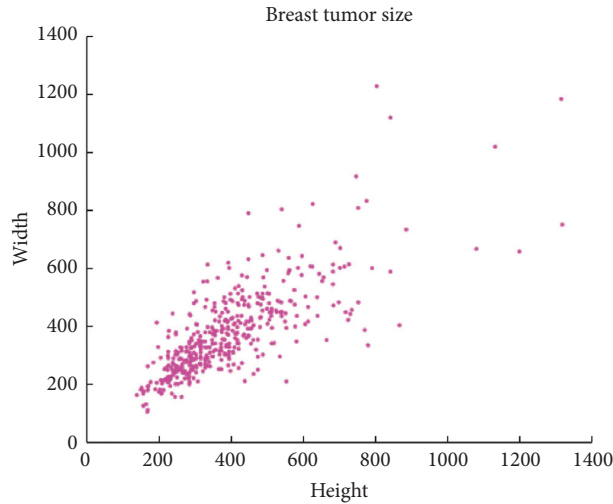


FIGURE 1: Breast tumours size in terms of width and height.

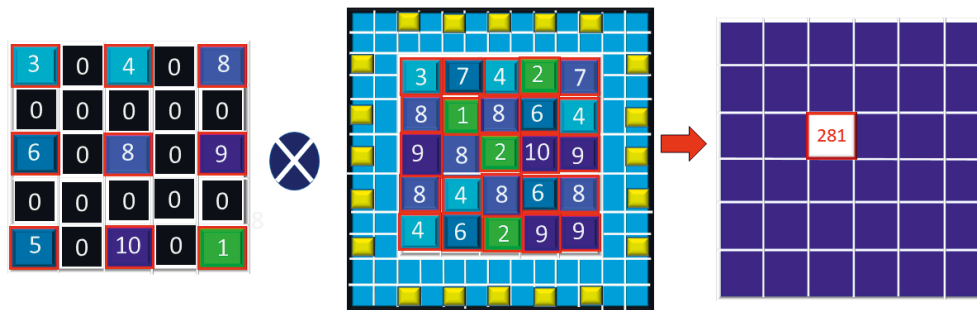


FIGURE 2: The atrous convolution layer.

them using parallel atrous convolutional layers. The item label is predicted by visual cues from various receptive fields.

There has been a lot of research done on machine and deep learning [18–23]. It is the categorisation and regression of the future. Smart applications need energy efficiency and security [24–26].

3. Proposed Model

We proposed an improved stochastic channel attention and a lightweight deep learning model for the detection and classification of breast cancer. An improved stochastic channel attention model is described in this study.

3.1. Improved Stochastic Channel Attention. The improved stochastic channel attention model employs normalised and augmented images to better identify small cells, which influences the feature extraction approach. As shown in Figure 3, a combination of maximum and stochastic pooling is used in this case [19]. Using maximum pooling may reveal single cancer cells. Each of the receptive fields picks a number. Stochastic pooling may be done in several ways. The dilation unit may employ stochastic pooling to process the feature map it generates. While the network’s depth

increases, the size of its filters decreases: 3×3 , 5×5 , 7×7 , and 9×9 squares.

The improved stochastic channel attention to get the most out of it is shown in Figure 3. The greatest results are obtained when improved stochastic channel attention is used in conjunction with DenseNet. This adds unnecessary expense by recalculating each dense block. Furthermore, each dream has its own unique focus. The improved stochastic channel attention might interfere with each dense block, reducing the model’s effectiveness. The channel attention mechanism chooses which components to focus on. However, not every channel aids in picture recognition [20]. The channel attention technique can help with malignant detection and family classification by looking at how many different channels there are. Most attention processes aim to improve performance. This adds unnecessary expense by recalculating each dense block. Furthermore, each dream has its own unique focus. The improved stochastic channel attention might interfere with each dense block, reducing the model’s effectiveness. The technique for creating each attention map is detailed below, as seen in Figure 4.

3.2. Proposed Lightweight Hybrid Dilated Ghost Model. For convolution and max pooling, the convolutional layer employs $96 \times 11 \times 11$ receptive filters with ReLu (LRN). Most

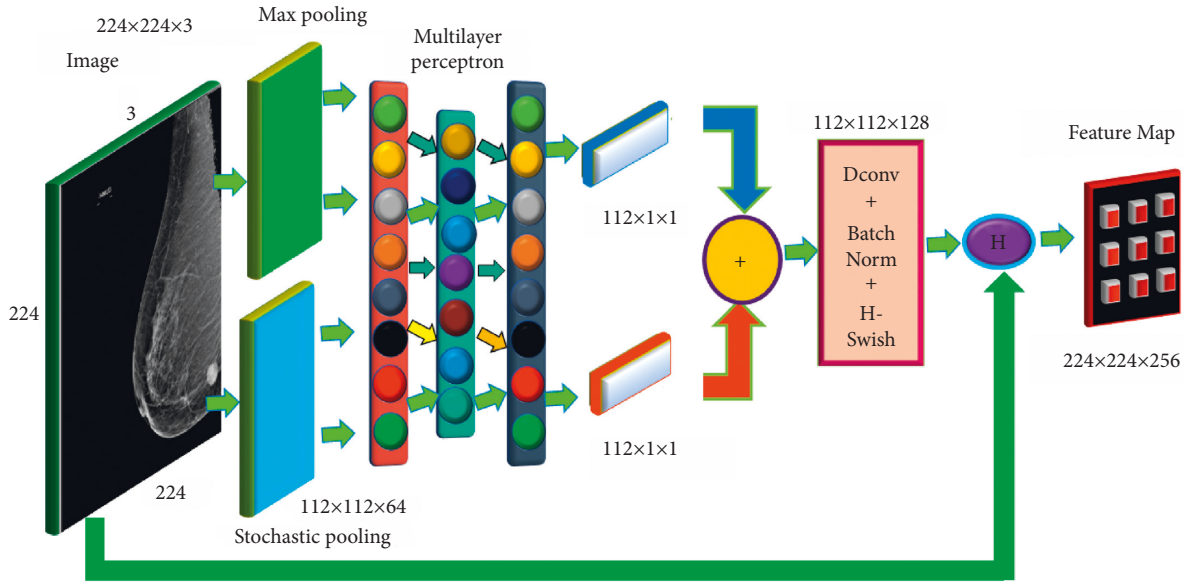


FIGURE 3: Improved stochastic channel attention model.

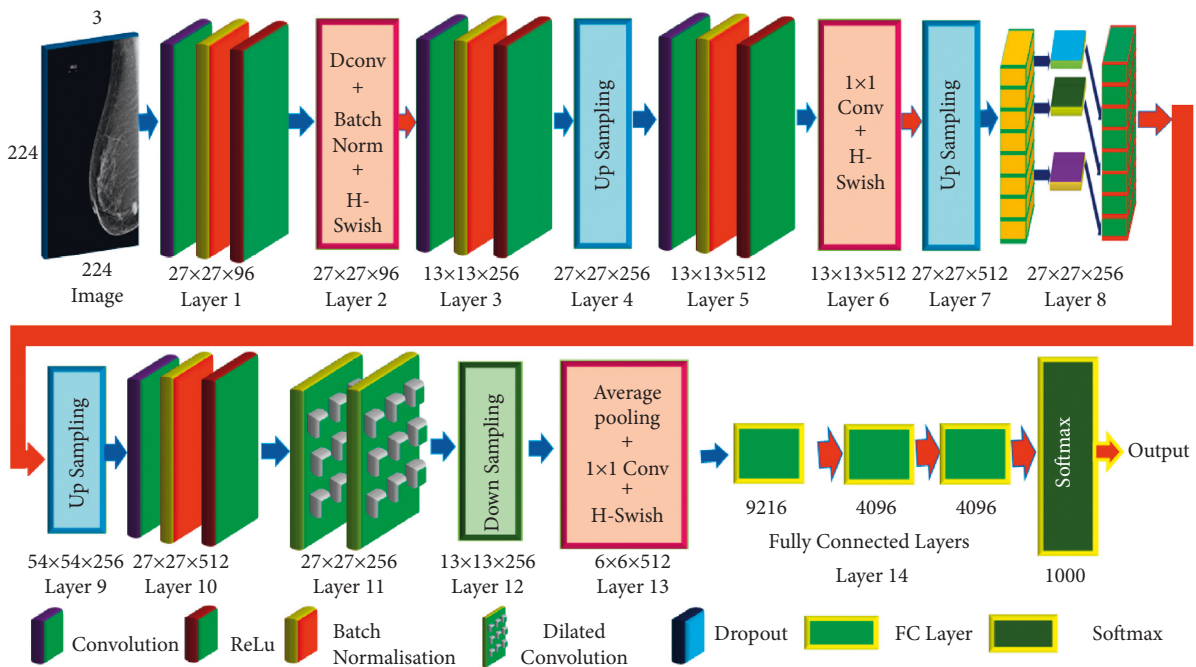


FIGURE 4: Proposed lightweight hybrid dilated ghost model.

pool systems need just three filters and two steps to be installed. In our experiments, the second layer of $27 \times 27 \times 96$ pixels may be employed. Replacing h-swish with a swish in quantitative mode increased the inference delay by 15% and improved the activation function of swish, although swish can be used to improve the accuracy [21]. Filters of size (5×5) is used as convolution kernels. The eighth and ninth layers were used to raster three feature maps. The characteristics of the previous layer are reversed and jumbled. Three-by-three filters with 512–256 feature maps are used in convolutional layers 5–13. A layer 6

picture may extract missing or additional features using a $13 \times 13 \times 512$ feature map. Pointwise convolutions are now employed before depth-wise convolutions when dealing with spatial data. Sandler proposed convolution is utilised in the ghost unit [22]. Convolutional layer data are often used in feature maps. There are various examples of overlap and resemblance in this congested system. Using flops and parameters to deal with many duplicate feature maps might be time-consuming. Take note of the lack of output in this scenario. The primary convolution kernel size of the ghost unit is as per Paoletti et al. [23]. Each feature map may be

utilised before the ghost module to conduct depth-wise convolution or shift. To preserve the underlying feature mapping, its identity is changed to a linear modification.

The improved stochastic channel attention model employs normalised and augmented images to better identify small cells, which influences the feature extraction approach. In order to extract unknown properties from the picture, the second layer of $27 \times 27 \times 96$ pixels may be employed. In our experiments, replacing h-swish with a swish in quantitative mode increased the inference delay by 15%. Swish has improved the activation function of swish, although swish can be used to improve the accuracy [21]. Pointwise convolutions are now employed before depth-wise convolutions when dealing with spatial data. Sandler proposed that convolution be utilised in the ghost unit [22]. Convolutional layer data are often used in feature maps. Each feature map may be utilised before the ghost module to conduct depth-wise convolution or shift. Now, the FC-DenseNet network has a deconvolution module, which is followed by a batch normalisation module and an *H*-swish module.

The goal of Layer 11 dilation convolution is to simplify the network. Minor cell analysis was aided by rapid feature conversions and 1×1 convolution components. This is a feature map with dimensions of $27 \times 27 \times 256$ pixels. Layer 2 down-sampling improves network performance. Neurons in neural networks may be destroyed, resulting in a reduced model. Layer 13 uses average pooling to reduce dimensions and retrieve information from several channels or feature maps. Layer 14 now features three FC levels. The FC layer links the other tiers together. Softmax activation in the FC layers transforms 9216 neurons into 1000 neurons. Due to the size of digital mammograms, several downsampling approaches are necessary to overfit the proposed model. It also needs a large amount of memory and computing power. As a result, we resized the picture. It is around 30 pixels in a 200-pixel tumour. FC-DenseNet excludes tiny tumours because of its pooling layers. Even when DenseNet upsampling and downsampling routes are merged, this influences the final segmentation accuracy. FC-DenseNet only downscales four times. The FC-DenseNet network now includes a deconvolution followed by batch normalisation and an *H*-swish module.

The channel attention mechanism chooses components to focus on. However, not every channel aids in picture recognition. Calculating distinct channels focuses the channel's attention on the most important areas of the picture. When attention is paid to the channels, they are able to improve malignant detection and family classification. Improved stochastic channel attention was used by SENet and CNN to improve their performance. Most attention processes aim to improve performance. The maximum pool, as opposed to the average pool, accumulates object attributes. Each of the average and maximum pools yields two geographic context descriptors (MC avg and MC max). In this step, a 1-dimensional convolution is conducted on two spatial context descriptors. Spatial attention, as opposed to channel attention, concentrates on a particular region of the feature detector. The spatial attention mechanism will concentrate on the map's most important aspects. Our ability to extract common malignant picture features and

categorise malignant families has increased. It combines the findings of the max and average pools to provide an informative feature descriptor. It is like group convolution in that it has the same number of groups as channels. Depth-wise convolution categorises input attributes based on channel count. SENet reduces local dimensionality and getting closer to each other on the channel axis could help you get more information from each channel.

3.3. Malignant Tumour Classification. Malignant detection and classification are covered in this article. An improved stochastic channel attention and DenseNet identify malignant cells using greyscale images. Greyscale images of known benign and harmful software samples with labels are used to train the model. The trained detection system can tell the difference between malicious and benign software. The malignant greyscale picture is used in the improved stochastic channel attention and DenseNet cancer family classification algorithms. Training images of known cancer families are utilised with labels identifying each cancer family. This approach has the potential to identify cancer and describes the whole procedure.

4. Experimental Results

4.1. Datasets. In this study, the dataset of Curated Breast Imaging Subset (CBIS)-DDSM was used [24]. Figure 4 depicts the CC and MLO perspectives on 190 separate mammography situations. As a result, 380 photographs were taken. DICOM grey-level digital mammography is used to make MLO and CC images. As shown in Figure 4, all mammography lesions were drawn by a hospital radiologist. The training, validation, and test sets are chosen at random. By contrast, the validation and test sets each had 75 images. Accuracy, recall, and the *F1* score are used in model detection and family categorisation. When classes are unequal, the accuracy rate reflects the total prediction level. It disregards the prediction abilities of some classes. Even if a few or major classes contain problems, classification accuracy may improve. This has been implemented via Python and an i7 system with 8 GB of RAM.

Table 1 shows each family's accuracy, recall, and *F1* scores. On the dataset, DenseNet has precision, 0.932 percent recall, and a 0.87 percent *F1* score. Improved stochastic channel attention does not increase CNN detection performance, even though the number of incorrect predictions in both trials is small. Our model beats current research based on existing research with an *F1* Score of 0.983, recall of 1, and precision of 0.975.

The standardised mammography pixel values are subtracted from the pixel mean values. The proposed model utilised different downsampling approaches to compare the two networks. Figure 5 depicts this for various tumour sizes. For all tumour sizes, the proposed model technique outperforms FC-DenseNet in terms of segmentation accuracy and edge retention. Merging multiscale picture data may assist in enhancing image segmentation performance that requires pixel-level semantic identification. The first two

TABLE 1: Performance of the proposed model.

Model	Malignant	Benign	Precision	Recall	F1 score
Proposed model	2105	784	0.975	1	0.983
DenseNet model	2084	645	0.932	0.87	0.935
DenseNet + CBAM model	1987	482	0.941	0.91	0.925
ResNet	2048	641	0.922	0.94	0.983
SDRG model	1989	589	0.956	0.91	0.965
DRGK model	2086	698	0.963	0.92	0.948

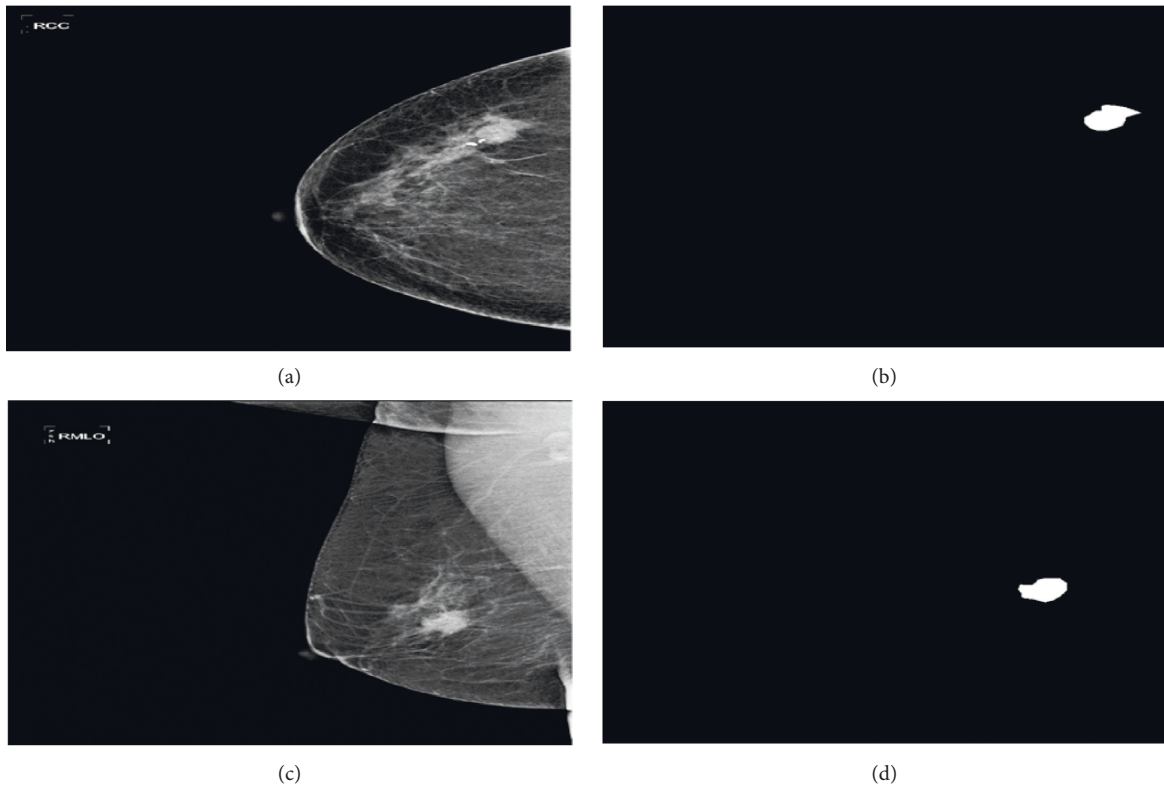


FIGURE 5: Segmented results of breast cancer.

mammography images discovered by FC-DenseNet contain modest variations in the inner and outer grey values. It may also validate the cancer segmentation capabilities of FC-breast DenseNet Table 2.

Table 3 displays the mean dice index, IOU, and pixel accuracy of the proposed model method. Even though the proposed model's dice index has gone up by 3.3 percentage points, the IOU has gone up by one percentage point, and the precision of pixels has remained almost exactly the same. They examine both false negatives and tumour pixel mis-detection rates, which may better indicate the algorithm's segmentation accuracy. Therefore, the proposed model therefore provides a competitive edge in terms of decreasing tumour pixel misdiagnosis.

Reducing the huge disparity in pixel counts is between the foreground (tumour) and backdrop. This loss model is less precise in determining the segmented tumour outline than the other two-loss models. The calculation of dice loss may influence gradient, training, and performance.

TABLE 2: The comparison of the dice index, intersection over union, and pixel accuracy of the proposed model with traditional models.

Methods	Dice index	Intersection over union	Pixel accuracy
DenseNet	72.63	61.57	84.21
SDRG model	74.95	62.58	78.34
Proposed model	82.98	71.35	81.29

TABLE 3: Quantitative comparisons using the proposed model.

Models	Dice index	IOU	Pixel accuracy
DenseNet	0.7355	0.5948	0.7868
Proposed model	0.7697	0.6041	0.7983

Figure 6 shows the tumour segmentation findings of many models. With great accuracy, the proposed model can separate tumours of diverse sizes and backgrounds. The

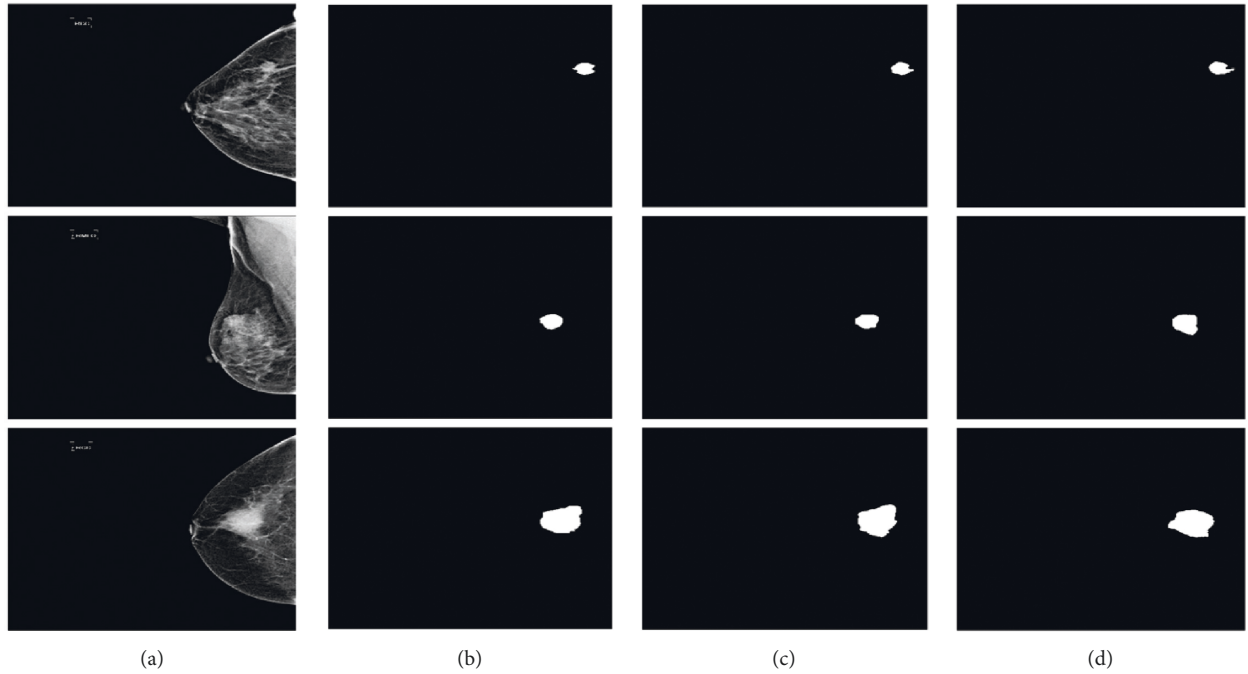


FIGURE 6: Breast tumours of various sizes are segmented. (a) Image; (b) DenseNet; (c) ResNet; (d) the proposed model.

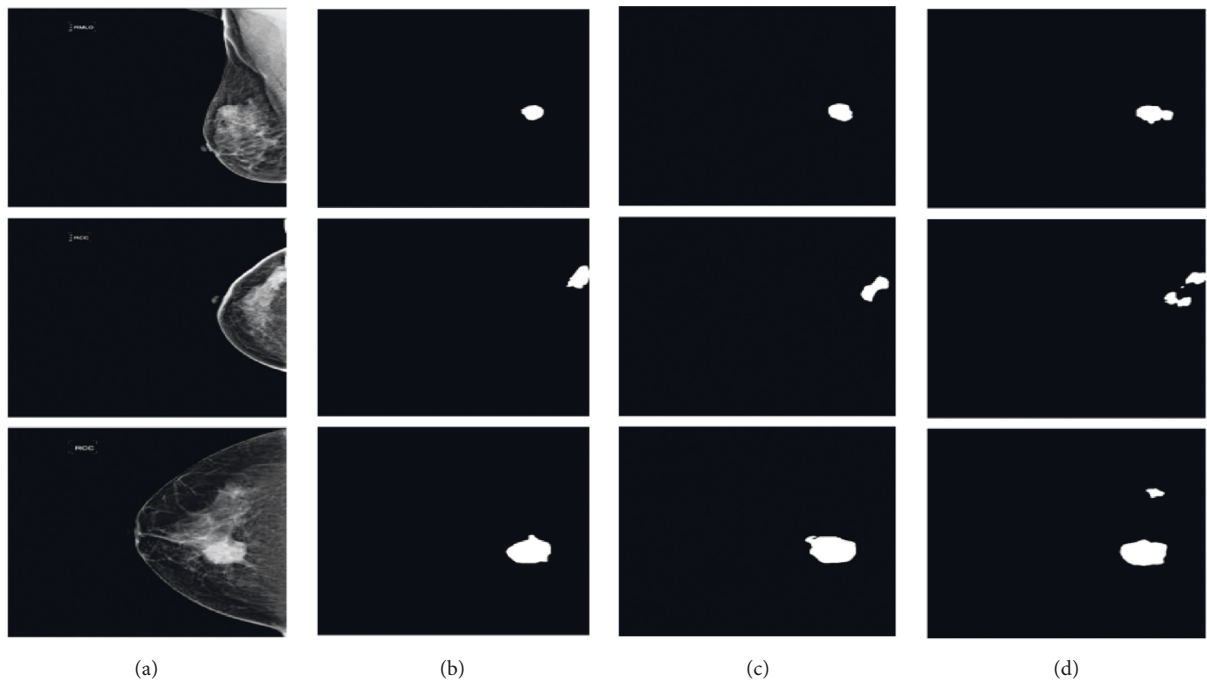


FIGURE 7: Different CNNs segmented tumours. (a) Image; (b) DenseNet; (c) DeepLab V3+ model; (d) the proposed model.

other two models were unable to get precise tumour borders. A significant number of false negatives were discovered. U-Net, DenseNet, and ResNet image segmentation models outperform U-Net. This shows the multiscale visual capabilities of the new ASPP module.

DeepLab V3+ model decoder module loses low-level information when using basic bilinear upsampling. Figure 7 shows different CNN segmented tumours: (a) DenseNet; (b)

DeepLab V3+ model; (c) the proposed model; and (d) to recover picture resolution and properties, our approach leverages U-Net decode and encode modules. As a result, it is more segregated. This is due to the proximity of the pectoralis grey value to the tumour. Figure 8 shows the first removal of the MLO pectoralis utilising location and grey threshold. The image segmentation method with threshold utilises two criteria to separate them. First, iterative

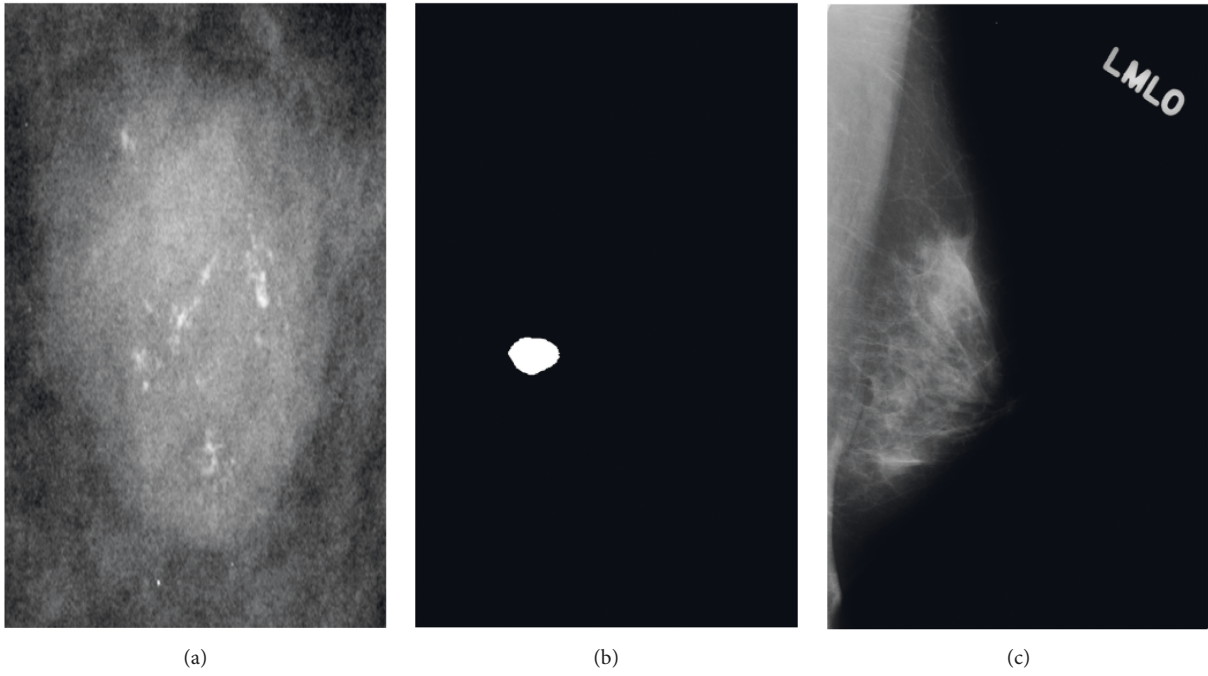


FIGURE 8: Deleted pectoralis from the original LMLO mammogram.

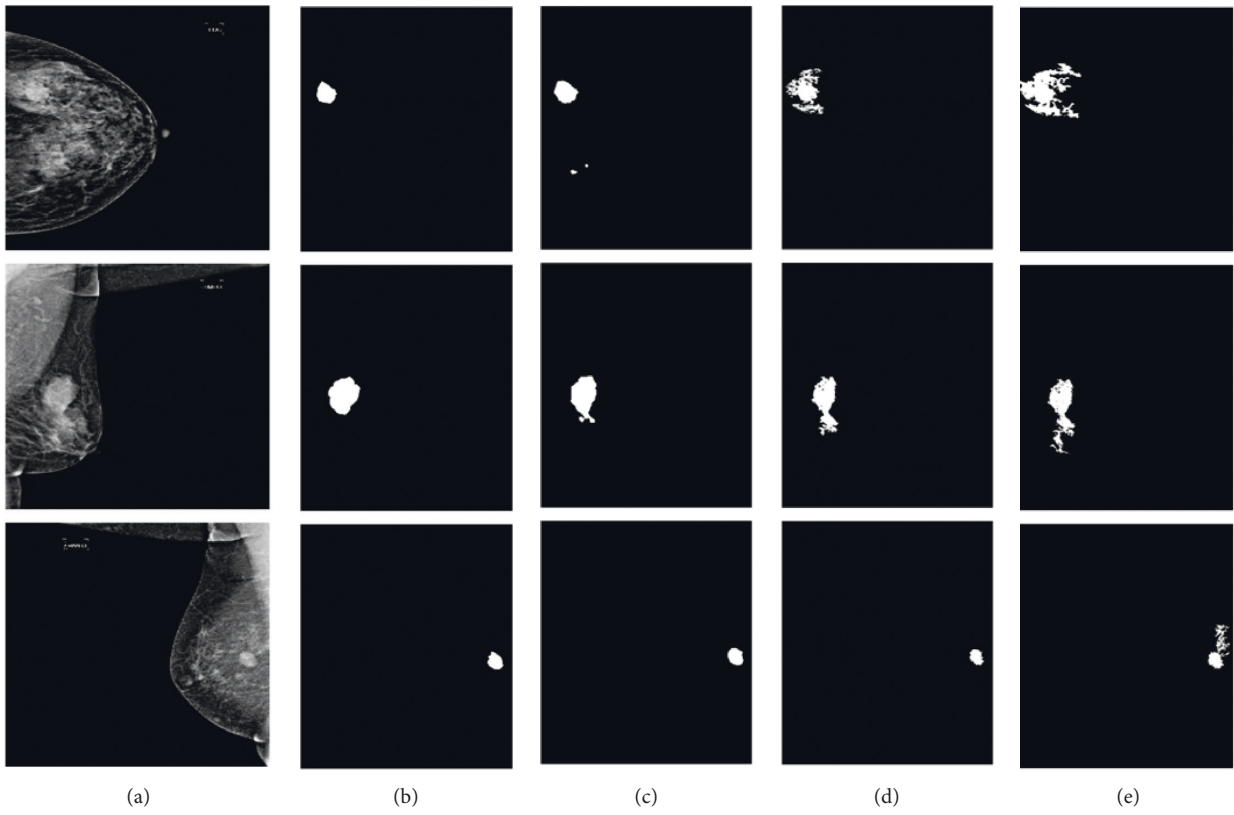


FIGURE 9: Results of comparison with other methods. (a) Image; (b) level-set method; (c) graph cut; (d) DenseNet; (e) the proposed model.

TABLE 4: The dice index, intersection over union, and pixel accuracy comparisons of the proposed model and traditional methods.

S.N.	Methods	Dice index	Intersection over union	Pixel accuracy
1	ResNet	0.5989	0.4893	0.6813
2	Grab cut	0.4663	0.3491	0.6220
3	Level set	0.5980	0.4587	0.6758
4	DenseNet	0.5464	0.4322	0.6440
5	The proposed model	0.7697	0.6041	0.7983

threshold segmentation is used to identify the first tumour area. The grey mean value of the first stage tumour segmentation is used in the final threshold segmentation. These three contrast methods do not include the little linked area in their results.

The proposed approach outperforms the previous three segmentation algorithms by deleting the pectoralis shown in Figure 8 for the LMLO mammogram. Less than 1% of images show minor alterations both within and outside the tumour. The greyscale, texture, and other characteristics of the tumour differentiate it from normal breast tissue. They employ the tumour’s greyscale and texture attributes rather than the image’s semantic information. These methods fail to distinguish nontumour regions that mimic tumours. Therefore, the suggested strategy enables more accurate segmentation. To be helpful, deep learning models must minimise both validation and training errors simultaneously. To attain this aim, it has been demonstrated that merging new data into existing data is a successful strategy. As a result, there will be less of a gap between training and validation datasets, and any future testing datasets created because of this. This also applies to any ensuing future testing datasets. While data augmentation is a strategy for reducing overfitting, alternative options were also investigated in this study. In the section that follows, we will look at several strategies for avoiding deep learning models from getting overfit. By reading on, readers will get a better idea of what data augmentation is all about. Figure 9 shows the results of tumour segmentation compared with other methods.

The number of false negative, false positive, true positive, and true negative samples together help to determine important classification parameters like precision, recall, and accuracy score. True negative and positive samples are denoted by TP and TN, respectively. The time required to extract, train, and test features is used to determine efficiency. Table 4 contains a comparison of the quantitative results. On all three assessment measures, it outperforms the previous three segmentation methods. The dice index, IOU, and pixel accuracy were all raised by 30% when the proposed model was used instead of the graph cut technique. Each of the three methods increased the dice index by 17.08 percent, above the specified threshold. Its accuracy has improved. Improved segmentation uses the dice index and IOU.

5. Conclusion

Breast tumours are automatically separated using the proposed lightweight deep learning model. The upsampling route in the proposed lightweight deep learning model may receive spatially detailed data from the downsampling channel. This

research shows how to automatically separate tumours in mammograms of different sizes and shapes. DenseNet detects malignancies and classifies families using the improved stochastic channel attention module. The recommended method for the family classification model converts executable files to greyscale images. In improved stochastic channel attention, a third less attention module option may improve model computational efficiency. Contrary to popular belief, the presented method detects malignant cells and classifies families. The lightweight techniques must comply with tougher execution, training, and energy limits in practice. It takes less time to extract features from a pretrained DenseNet-121 model than it does to train a CNN model from scratch. DenseNet detects malware and classifies families using the improved stochastic channel attention. The suggested technique turns executable files into greyscale pictures, which are then used to identify malware families via the family classification model. It also outperforms improved stochastic channel attention, helping CNN. Even though there are problems with code and class imbalance, the proposed method works well at finding malware and classifying families. Segmentation and classifiers may both be improved; the proposed method does not process the malware’s initial greyscale image in the model. Research can be carried out to investigate these problems and enhance performance. To autonomously distinguish breast tumours, the proposed lightweight deep learning model uses multiscale visual information. Following the final downsampling, the network receives the atrous spatial pyramid pooling module, which combines several fields of view of image attributes through atrous convolution sampling rates. This research shows how to automatically separate tumours in mammograms of different sizes and shapes. It is expected that adding more data and learning in different domains, such as the frequency domain, and using new architectural designs, such as graph convolutional networks, will make their performance much better. The appropriateness and acceptability of categorisation and discrimination measures should be explained in model performance reports in future. Finally, we include information on how the model was reviewed and verified, and how missing values and outliers were handled.

Data Availability

In this study, dataset of Curated Breast Imaging Subset (CBIS)-DDSM is used. The dataset is downloaded from website: <https://www.kaggle.com/datasets/awsaf49/cbis-ddsm-breast-cancer-image-dataset?resource=download>. [Accessed: 14-Apr-2022]. The data are available from the corresponding author upon request.

Conflicts of Interest

The authors declare that they have no conflicts of interest.

References

- [1] D. Vasan, M. Alazab, S. Venkatraman, J. Akram, and Z. Qin, "MTHAEL: cross-architecture IoT malware detection based on neural network advanced ensemble learning," *IEEE Transactions on Computers*, vol. 69, no. 11, pp. 1654–1667, 2020.
- [2] A. Sahakyan and H. Sarukhanyan, "Segmentation of the breast region in digital mammograms and detection of masses," *International Journal of Advanced Computer Science and Applications*, vol. 3, no. 2, 2012.
- [3] R. Kashyap and V. Tiwari, "Energy-based active contour method for image segmentation," *International Journal of Electronic Healthcare*, vol. 9, no. 2/3, p. 210, 2017.
- [4] V. Tiwari and R. Kashyap, "Active contours using global models for medical image segmentation," *International Journal of Computational Systems Engineering*, vol. 4, no. 2/3, p. 195, 2018.
- [5] S. Hong, S. Kwak, and B. Han, "Weakly supervised learning with deep convolutional neural networks for semantic segmentation: understanding semantic layout of images with minimum human supervision," *IEEE Signal Processing Magazine*, vol. 34, no. 6, pp. 39–49, 2017.
- [6] Q. Zhou, W. Zhu, F. Li, M. Yuan, L. Zheng, and X. Liu, "Transfer learning of the ResNet-18 and DenseNet-121 model used to diagnose intracranial hemorrhage in CT scanning," *Current Pharmaceutical Design*, vol. 28, no. 4, pp. 287–295, 2022.
- [7] Y. Wang, S. Wang, J. Chen, and C. Wu, "Whole mammographic mass segmentation using attention mechanism and multiscale pooling adversarial network," *Journal of Medical Imaging*, vol. 7, no. 5, Article ID 54503, 2020.
- [8] A. Krizhevsky, I. Sutskever, and G. E. Hinton, "ImageNet classification with deep convolutional neural networks," *Communications of the ACM*, vol. 60, no. 6, pp. 84–90, 2017.
- [9] R. Nair, S. Vishwakarma, M. Soni, T. Patel, and S. Joshi, "Detection of COVID-19 cases through X-ray images using hybrid deep neural network," *World Journal of Engineering*, vol. 19, no. 1, pp. 33–39, 2021.
- [10] T. Sharma, R. Nair, and S. Gomathi, "Breast cancer image classification using transfer learning and convolutional neural network," *IJMOR*, vol. 2, no. 1, pp. 8–16, 2022.
- [11] M. S. Majib, M. M. Rahman, T. M. S. Sazzad, N. I. Khan, and S. K. Dey, "VGG-SCNet: a vgg net-based deep learning framework for brain tumor detection on mri images," *IEEE Access*, vol. 9, Article ID 116942, 2021.
- [12] V. Badrinarayanan, A. Kendall, and R. Cipolla, "SegNet: a deep convolutional encoder-decoder architecture for image segmentation," *IEEE Transactions on Pattern Analysis and Machine Intelligence*, vol. 39, no. 12, pp. 2481–2495, 2017.
- [13] N. Ibtihaz and M. S. Rahman, "MultiResUNet: rethinking the U-Net architecture for multimodal biomedical image segmentation," *Neural Networks*, vol. 121, pp. 74–87, 2020.
- [14] J. Hai, K. Qiao, J. Chen et al., "Fully convolutional DenseNet with multiscale context for automated breast tumor segmentation," *Journal of Healthcare Engineering*, vol. 2019, Article ID 8415485, 11 pages, 2019.
- [15] Z. Wang, X. Li, M. Yao, J. Li, Q. Jiang, and B. Yan, "A new detection model of microaneurysms based on improved FC-DenseNet," *Scientific Reports*, vol. 12, no. 1, p. 950, 2022.
- [16] S. Nandhini and K. Ashokkumar, "An automatic plant leaf disease identification using DenseNet-121 architecture with a mutation-based henry gas solubility optimization algorithm," *Neural Computing & Applications*, vol. 34, no. 7, pp. 5513–5534, 2022.
- [17] R. Kashyap, "Breast cancer histopathological image classification using stochastic dilated residual ghost model," *International Journal of Information Retrieval Research*, vol. 12, no. 1, pp. 1–24, 2022.
- [18] R. Nair, A. Alhudhaif, D. Koundal, R. I. Doewes, and P. Sharma, "Deep learning-based COVID-19 detection system using pulmonary CT scans," *Turkish Journal of Electrical Engineering and Computer Sciences*, vol. 29, no. 8, pp. 2716–3243, 2021.
- [19] R. Kashyap, "Evolution of histopathological breast cancer images classification using stochastic dilated residual ghost model," *Turkish Journal of Electrical Engineering and Computer Sciences*, vol. 29, no. 8, pp. 2758–2840, 2021.
- [20] A. Tavares da Silva and C. Roberto Siebert, "DenseNet-DC: optimizing DenseNet parameters through feature map generation control," *Revista de Informática Teórica e Aplicada*, vol. 27, no. 3, pp. 25–39, 2020.
- [21] H. H. Chieng, N. Wahid, O. Pauline, and S. R. K. Perla, "Flatten-T Swish: a thresholded ReLU-Swish-like activation function for deep learning," *International Journal of Advances in Intelligent Informatics*, vol. 4, no. 2, p. 76, 2018.
- [22] M. Sandler, A. Howard, M. Zhu, A. Zhmoginov, and L. Chen, "MobileNetV2: inverted residuals and linear bottlenecks," in *Proceedings of the 2018 IEEE/CVF Conference on Computer Vision and Pattern Recognition*, Salt Lake City, UT, USA, June 2018.
- [23] M. E. Paoletti, J. M. Haut, N. S. Pereira, J. Plaza, and A. Plaza, "Ghostnet for hyperspectral image classification," *IEEE Transactions on Geoscience and Remote Sensing*, vol. 59, no. 12, Article ID 10378, 2021.
- [24] Cbis-Ddsm, "Breast cancer image dataset," Kaggle.com, 2022, <https://www.kaggle.com/datasets/awsaf49/cbis-ddsm-breast-cancer-image-dataset?resource=download>.
- [25] C. Sushovan, S. Nilesh, S. Kartik, B. Prasanalakshmi, and M. Shabaz, "A novel approach to classifying Breast cancer histopathology biopsy images using bilateral knowledge distillation and label smoothing regularization," *Computational and Mathematical Methods in Medicine*, vol. 2021, Article ID 4019358, 11 pages, 2021, <https://doi.org/10.1155/2021/4019358>.
- [26] C. Sushovan, M. Rakhra, N. Memon, S. Kartik, and M. Teshome Ayana, "Breast cancer calcifications: identification using a novel segmentation approach," *Computational and Mathematical Methods in Medicine*, vol. 2021, Article ID 9905808, 13 pages, 2021, <https://doi.org/10.1155/2021/9905808>.